Concave Fe_2O_3 Nanocubes with High-index Facets for Ammonia Production from Electrocatalytic Nitrate Reduction

Yuwei Zhang, Mingyang Xu, Jiaxin Zhou, Fen Yao, Hanfeng Liang*

Experimental section

Materials. Carbon papers (CPs, TGP-H-060, 0.19 mm thickness), Zn foils (0.2 mm thickness) and Dupont proton exchange membranes (Nafion N115) were purchased from Suzhou Sinero Technology Co. Ltd. Potassium hydroxide (KOH, AR),sodium hydroxide (NaOH, AR), ferric nitrate hydrate ($Fe(NO_3)_3·9H_2O$, AR), copper acetate ($CuOAc_2·H_2O$), potassium nitrate (KNO_3, AR), ferric chloride ($FeCl_3$, AR), sodium bicarbonate ($NaHCO_3$, AR), Nitric acid (KNO_3, AR), Sodium Carbonate (Na_2CO_3, AR), Phosphoric acid (H_3PO_4, AR) were purchased from Sinopharm Chemical Reagent Co., Ltd. $NH_3·H_2O$ (25 *wt.*%) , hydrazine hydrate ($N_2H_4·H2O$, 85%), ammonia and nitrate standard solutions were obtained from Shanghai Macklin Biochemical Co., Ltd. Dupont proton exchange membrane (PEM, Nafion N115) and 5 wt% Nafion solution were purchased from Suzhou Sinero Technology Co. Ltd. The distilled water (10-15 MΩ·cm) used throughout all experiments was purified through a Millipore system.

Preparation of H_o-Fe_2O_3. 2 mmol of $Fe(NO_3)_3·9H_2O$ and 1 mmol of $CuOAc_2·H_2O$ were dissolved in 10 mL of deionized water to form a homogeneous solution followed by ultrasonic treatment for 10 min. Then 10 mL of $NH_3·H_2O$ (25 *wt.*%) was added into the solution. After irradiated by ultrasonic waves for another 5 min, the mixture was transferred into a Teflon-lined stainless-steel autoclave of 50 mL capacity, sealed and maintained at 140 °C for 20 h. After the mixture was cooled to room temperature naturally, the obtained product was collected and washed several times with deionized water and ethanol, and finally dried at 60 °C for 12 h.

Preparation of L_o-Fe_2O_3. 2 mmol of $Fe(NO_3)_3·9H_2O$ was dissolved in 10 mL of deionized water to form a homogeneous solution followed by ultrasonic treatment for 10 min. Then 10 mL of $NH_3·H_2O$ (25 *wt.*%) was added into the solution. After irradiated by ultrasonic waves for another 5 min, the mixture was transferred into a Teflon-lined stainless steel autoclave of 50 mL capacity, sealed and maintained at 140 °C for 20 h. After the mixture was cooled to room temperature naturally, the obtained product was collected and washed several times with deionized water and ethanol, and finally dried at 60 °C for 12 h.

Preparation of L_c-Fe_2O_3. 20 mL of 5.4 mol L^{-1} NaOH and 2 mol L^{-1} $FeCl_3$ mixed solution stirred for 10 min at 75°C. The mixture was transferred into a Teflon-lined stainless steel autoclave of 50 mL capacity, sealed and maintained at 100 °C for 4days. After the mixture was cooled to room temperature naturally, the obtained product was collected and washed several times with deionized water and ethanol, and finally dried at 60 °C for 12 h.

Preparation of H_o-Fe_2O_3, L_o-Fe_2O_3, L_c-Fe_2O_3 on carbon paper. 2 mg H_o (L_o, L_c)-Fe_2O_3 powder was dispersed in a mixed solution containing 100 μL distilled water, 100 μL isopropanol and 10 μL 5 wt% Nafion solution with an ultrasonic powder of 40 kHz for at least 1 h to form the homogeneous ink. The whole ink was then drop-casted onto a piece of carbon paper (1 cm × 1 cm) under the infrared heating lamp.

Physical characterization. Scanning electron microscopy (SEM) images were recorded on a HITACHI S-4800. Transmission electron microscopy (TEM) images were collected on a JEM-1400. X-ray diffraction (XRD) patterns were recorded by Rigaku Ultima-IV XRD with Cu-Kα radiation (λ = 1.5405 Å). X-ray photoelectron spectroscopy (XPS) analysis was performed on Thermo Fisher ECSALAB Xi+ with Al-Kα as radiation source. Ammonia and nitrite concentrations were determined by a 850 professional ion chromatography (IC). Raman test was conducted on a Renishaw in Via confocal Raman microscope under an excitation of 532 nm laser with the power of 0.04 mW. FTIR spectroscopy test was conducted on a Nicolet iS50 FTIR spectroscopy.

Electrochemical test. Nitrate reduction reaction (NtrRR) was tested via a Chenhua electrochemical workstation (CHI660E) in a H-type electrolytic cell, wherein a Carbon parper with catalyst loading, a Pt sheet and a Hg/HgO electrode were used as working, auxiliary and reference electrodes, respectively. Anolyte was 1 M KOH while catholyte was 1 M KOH/0.1M KNO_3 mixed solution. They were separated by a Nafion 115 PEM. The catholyte was continuously stirred with 1000 rpm throughout the tests to minimize mass transport limits. All the linear sweep voltammetry (LSV) curves were recorded at 5mV s^{-1}, and all the potentials were converted into reversible hydrogen potential (RHE) by Nernst equation with iRs compensation by the following formula.

$$E \textit{ vs. } RHE = E \textit{ vs. } HgO/Hg + 0.0592 \times pH + 0.098\ V - iRs$$

where Rs is the solution impedance, obtained by the impedance tests. Chronoamperometry and chronopotentiometry were conducted to evaluate the NtrRR Faradaic efficiency and stability. The electrolytes after tests were injected into IC to measure the ammonia and nitrite concentrations. The Faradaic efficiency of ammonia or nitrite production and the ammonia production rate were calculated as follows.

$$\text{Faradic efficiency: } FE = nzF/It \times 100\% \quad (1)$$

$$\text{Ammonia production rate: } Q = n/At \quad (2)$$

where n, z, F, i, t and A are moles of products (mol), transferred electron number (2 for nitrite or 8 for ammonia), Faraday constant (96485 C mol^{-1}), current (A), time (s) and geometric area of electrodes (cm^2), respectively.

Hydrogen evolution reaction (HER) tests were also conducted in the same H-type electrolytic cell except that the catholyte was replaced by 50 mL of 1 M KOH. Polarization curves were collected in the same way.

Assembly of batterolyzers. The N_2H_4-nitrate batterolyzer was assembled in a membrane electrode flow reactor, wherein the *Ho*-Fe_2O_3 on carbon paper (2 cm × 2cm) was used as the cathode, and the RuO_x on carbon paper (2 cm × 2 cm) was used as the anode, respectively. They were separated by a K^+ exchange membrane (transformed from a Nafion N115 PEM). Catholyte was 1 M KOH/0.1 M KNO_3 while anolyte was 1 M KOH/0.1 M N_2H_4, and their flow rates were controlled to be 150 mL min^{-1} by a peristaltic pump. Two pieces of TA1-type titanium metal, engraved with single serpentine flow channel, were used as bipolar plates. Chronopotentiometry was employed to evaluate the stability. Discharging power densities were equal to current densities times voltages.

Determination of ammonia and nitrite using IC. In this work, the concentrations of the ammonia and nitrite in the electrolyte were quantified by IC, unless otherwise specified. The electrolyte solution was diluted and then directly injected into the IC to measure their concentrations. The standard curves were plotted by diluted standard solution against the peak area of ionic conductivity (Fig. S6, ESI†). The chromatographic filtrate was 5 vol% HNO_3 for cation detection or 1 mM $NaHCO_3$ and 3 mM Na_2CO_3

mixed solution for anion detection. The solution for suppressor was 1 vol% H_3PO_4.

Additional figures

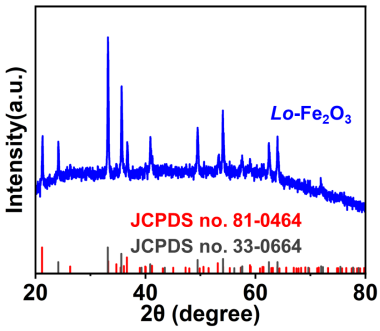

Fig. S1 XRD patterns of *Lo*-Fe_2O_3.

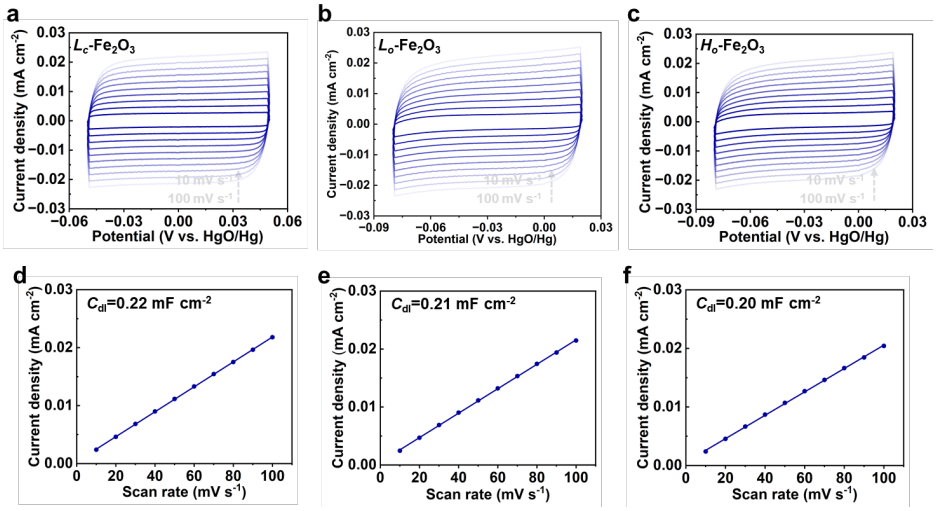

Fig. S2 (a, b, c) CV curves within non-Faradaic regions and (d, e, f) the calculated specific C_{dl} of the *Ho*-Fe_2O_3, *Lo*-Fe_2O_3 and *Lc*-Fe_2O_3 catalysts.

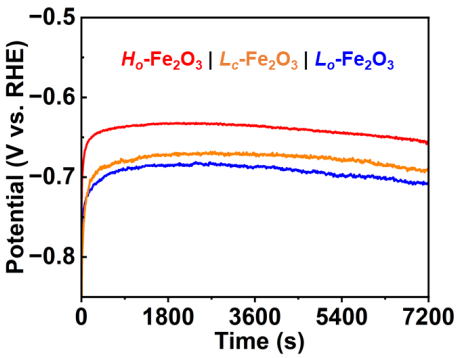

Fig. S3 Chronopotentiometry curves of *Ho*-Fe_2O_3, *Lo*-Fe_2O_3 and *Lc*-Fe_2O_3 under -250 mA cm^{-2} for 7200 s in a 1 M KOH/0.1 M KNO_3 mixed electrolyte.

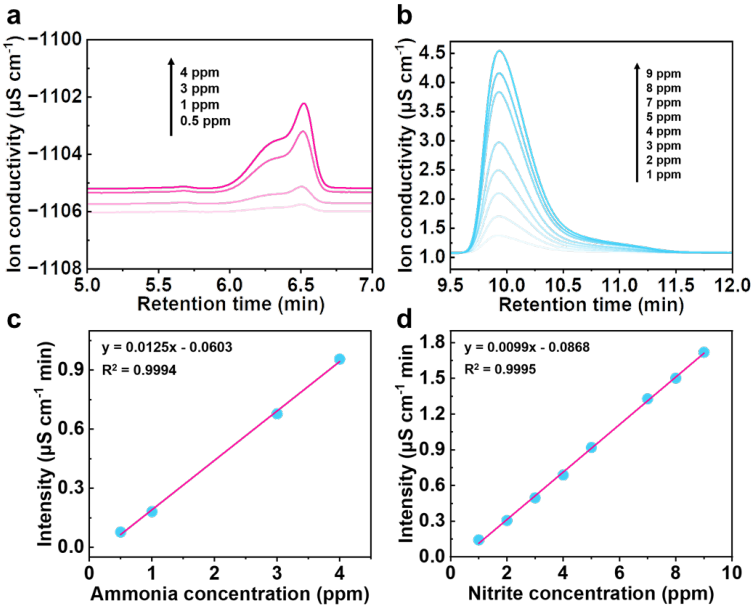

Fig. S4 (a, b) IC signal curves and (c, d) plotted standard curves of ammonia and nitrite, respectively.

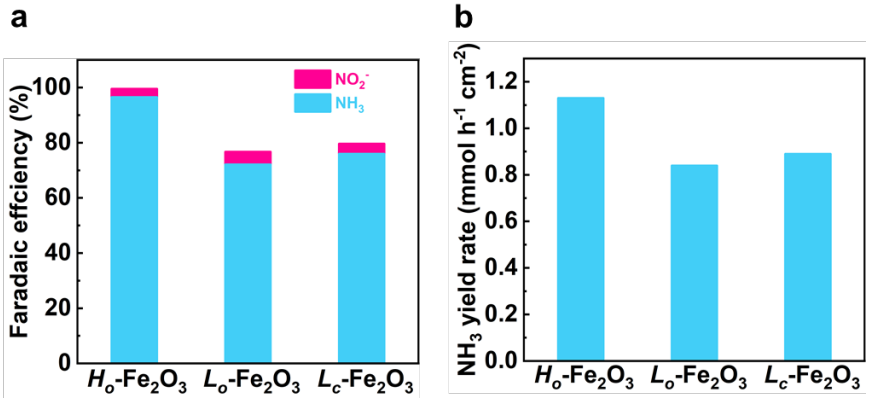

Fig. S5 (a) Ammonia Faradaic efficiencies, (b) Ammonia yield rates under 250 mA cm^{-2}.

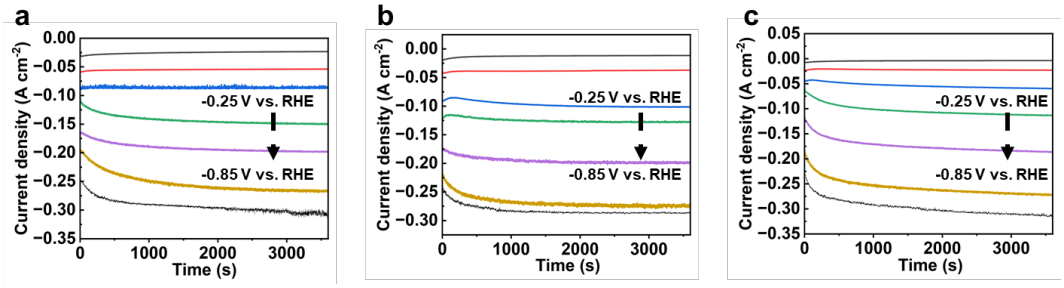

Fig. S6 (a, b, c) Chronoamperometry curves of the H_o-Fe_2O_3, L_o-Fe_2O_3 and L_c-Fe_2O_3 under different potentials.

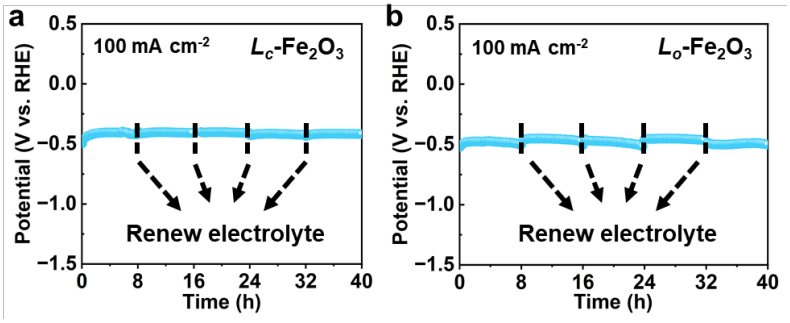

Fig. S7 Chronopotentiometry curves of the (a) L_c-Fe_2O_3 and (b) L_o-Fe_2O_3 catalyst at 100 mA cm^{-2} in a 1 M KOH/0.1 M KNO_3 mixed electrolyte.

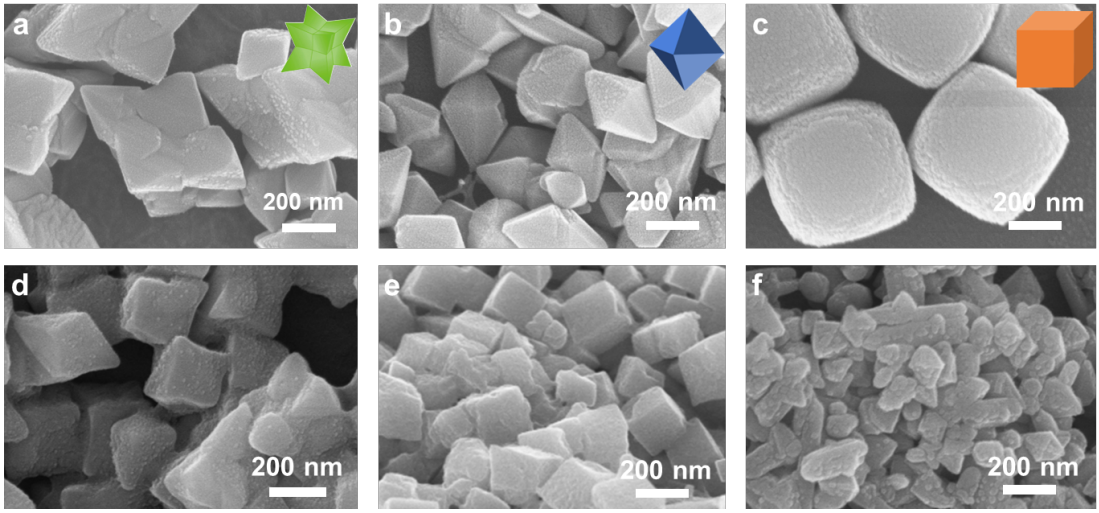

Fig. S8 (a, b, c) SEM images of H_o-Fe_2O_3, L_o-Fe_2O_3, Lc-Fe_2O_3 before long-term stability tests. (d, e, f) SEM images of H_o-Fe_2O_3, L_o-Fe_2O_3, Lc-Fe_2O_3 after long-term stability tests.

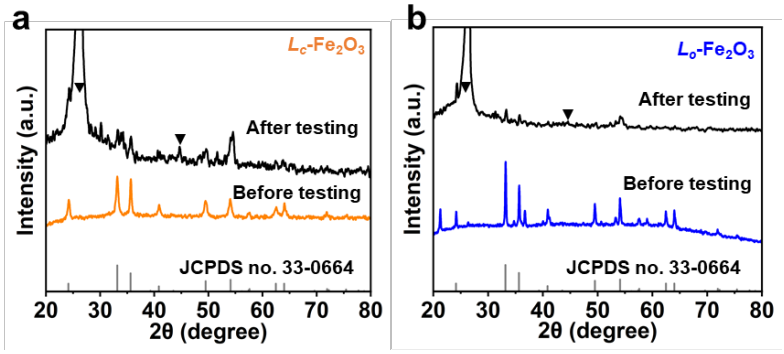

Fig. S9 (a,b) XRD patterns of L_c-Fe_2O_3 and L_o-Fe_2O_3, respectively.

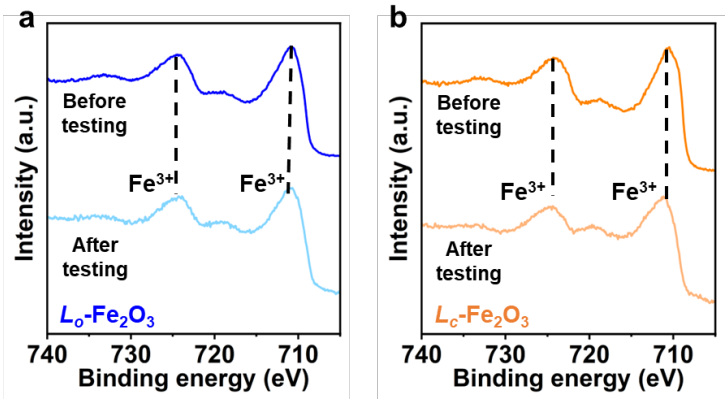

Fig. S10 Fe 2p XPS spectra of the (a) *Lo*-Fe_2O_3, (b) *Lc*-Fe_2O_3 before and after the long-term stability tests.

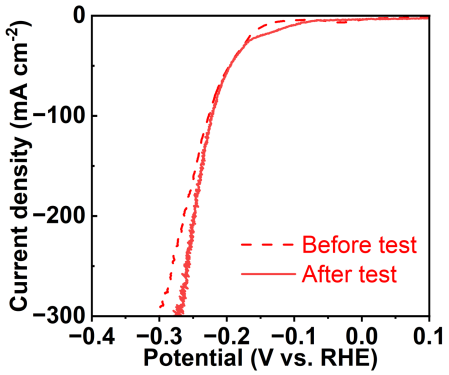

Fig. S11 Polarization curves in 1 M KOH/0.1 M KNO_3 of *Ho*-Fe_2O_3 before (dotted line) and after (solid line) stability tests (with *IR* correction).

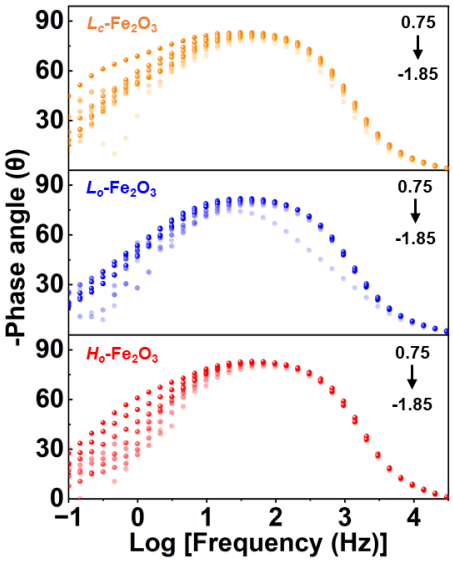

Fig. S12 Bode phase plots of *Ho*-Fe_2O_3, *Lo*-Fe_2O_3 and *Lc*-Fe_2O_3 at various potentials.

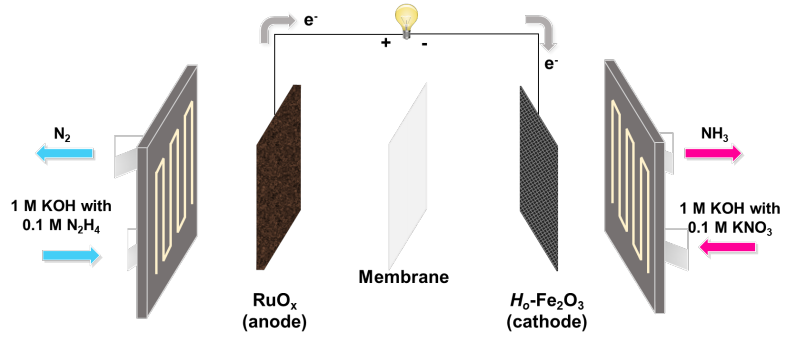

Fig. S13 Illustration of the membrane electrode assembly of the N_2H_4-nitrate batterolyzer.

Table S1 Comparison of NtrRR performance of the H_o-Fe_2O_3 with other recently reported catalysts.

Catalyst	Potential (V *vs.* RHE) @10 mA cm^{-2}	Ammonia Faradaic efficiency (%)	Ammonia yield (mmol h^{-1} cm^{-2})	Reference
H_o-Fe_2O_3	-0.15	96.54	1.13	This work
FeP_2	-0.5	91.4	0.105	[1]
FeCoNiAlTi	0.52	95.23	-0.55	[2]
Fe_2O_3 NRs	-0.6	75	0.328	[3]
Co_3O_4/Co	-0.4	88.7	0.26	[4]
FeOOH	-0.5	92	0.142	[5]
Cu/Cu_2O NWAs	-0.25	95.8	0.2449	[6]
CuPc@MXene	-0.8	94	0.02	[7]
B-MoS_2	-0.35	92.3	0.635	[8]
Pd/NF	-0.45	78%	1.52	[9]
$NiCo_2O_4$	-0.25	92.42	0.038	[10]

Table S2 Rs, Rct and CPE1 data obtained after fitting Nyquist plots for NtrRR

catalyst	Rs (Ω)	Rct (Ω)	CPE1 (Ω)
Ho-Fe_2O_3	1.18	0.51	0.047371
Lo-Fe_2O_3	1.18	0.51	0.046232
Lc-Fe_2O_3	1.56	0.94	0.029288

References

1. Z. Hou, Y. Zhang, H. Chen, J. Wang, A. Li and P. François‐Xavier Corvini, Small, 2406424.

2. R. Zhang, Y. Q. Zhang, B. Xiao, S. C. Zhang, Y. B. Wang, H. L. Cui, C. Li, Y. Hou, Y. Guo, T. Yang, J. Fan and C. Y. Zhi, *Angew. Chem.-Int. Edit.*, 2024, e202407589.

3. T. S. Li, C. Tang, H. Guo, H. R. Wu, C. Duan, H. Wang, F. Y. Zhang, Y. H. Cao, G. D. Yang and Y. Zhou, *ACS Appl. Mater. Interfaces*, 2022, **14**, 49765-49773.

4. F. L. Zhao, G. T. Hai, X. Li, Z. Y. Jiang and H. H. Wang, *Chem. Eng. J.*, 2023, **461**, 10.
5. Q. Liu, Q. Liu, L. S. Xie, Y. Y. Ji, T. S. Li, B. Zhang, N. Li, B. Tang, Y. Liu, S. Y. Gao, Y. L. Luo, L. M. Yu, Q. Q. Kong and X. P. Sun, *ACS Appl. Mater. Interfaces*, 2022, **14**, 17312-17318.
6. Y. T. Wang, W. Zhou, R. R. Jia, Y. F. Yu and B. Zhang, *Angew. Chem.-Int. Edit.*, 2020, **59**, 5350-5354.
7. L. X. Li, W. J. Sun, H. Y. Zhang, J. L. Wei, S. X. Wang, J. H. He, N. J. Li, Q. F. Xu, D. Y. Chen, H. Li and J. M. Lu, *J. Mater. Chem. A*, 2021, **9**, 21771-21778.
8. Y. J. Luo, K. Chen, P. Shen, X. C. Li, X. T. Li, Y. H. Li and K. Chu, *J. Colloid Interface Sci.*, 2023, **629**, 950-957.
9. H. Guo, M. Y. Li, Y. T. Yang, R. Luo, W. Liu, F. Y. Zhang, C. Tang, G. D. Yang and Y. Zhou, *Small*, 2022, **19**, 11.
10. W. X. Tao, P. F. Wang, B. Hu, X. Wang and G. Zhou, *J. Environ. Chem. Eng.*, 2023, **11**, 9.